



## Lumped-parameter equivalent circuit modeling of solar cells with S-shaped I-V characteristics

Fei Yu<sup>a,\*</sup>, Gongyi Huang<sup>a</sup>, Wei Lin<sup>a</sup>, Chuanzhong Xu<sup>a</sup>, Wanling Deng<sup>b</sup>, Xiaoyu Ma<sup>b</sup>, Junkai Huang<sup>b</sup>

<sup>a</sup> College of Information Science and Engineering, Huaqiao University, Xiamen 361021, China

<sup>b</sup> Department of Electronic Engineering, Jinan University, Guangzhou 510630, China



### ARTICLE INFO

The review of this paper was arranged by Prof. Y. Kuk

**Keywords:**  
Solar cells  
Lumped-parameter equivalent circuit model  
I-V characteristics  
S-shaped kink

### ABSTRACT

In this paper, we propose a method to analytically solve some types of DC lumped-parameter equivalent circuit models for solar cells with S-shaped *I*-*V* characteristics measured under illumination. Based on the models proposed previously by other authors, we present the set of equations describing solar cell's terminal current and voltage, derive the analytical solutions of *I*-*V* characteristics, and give discussions about the effects from the model parameters on solar cells' *I*-*V* characteristics. The comparisons between the proposed solutions and the least square method results illustrate that the solution calculation scheme is not only both accurate and efficient, but also valid in the whole operation regime of solar cells especially for the S-shaped kink in the first quadrant. Finally, the solutions are validated by the reconstructed experimental data to demonstrate that they can be adopted in the practical applications of solar cells. As a result, the feature of the proposed solutions can decrease computation complexity, ease the extraction process of the solar cells' model fitting parameters, and increase simulation accuracy.

### 1. Introduction

Recently, many kinds of new generation solar cells are undergoing the intensive researches for innovative developments, further experiments, and practical photovoltaic applications. These new generation solar cells include non-crystalline hetero-junction solar cells [1], silicon quantum dot solar cells [2], perovskite semiconductor solar cells [3,4], organic semiconductor-based solar cells [5,6], and so on. Among all of these above solar cells, i.e., the most promising candidates for the next generation photovoltaic devices, the S-shaped *I*-*V* characteristics show up under the dark and illumination conditions and impair energy conversion capacity because of the decrease of the fill factor [7]. Especially, the presence of the anomalous S-shaped kink [8] at large forward voltages in the first quadrant of the *I*-*V* characteristics, resulting from contact and other interface phenomena [9], must be minimized or suppressed [10].

Compared with the conventional solar cell lumped-parameter models [11], more suitable specialized lumped-parameter equivalent circuit models [7,12–17] are introduced to specifically represent the S-shaped *I*-*V* characteristics of solar cells by adding an additional sub-circuit, which are regarded as a tool for analysis of the effects from the

processes, materials, and operating conditions on the S-shaped *I*-*V* characteristics of solar cells. Unfortunately, an analytical solution for the terminal current as a function of the terminal voltage is not feasible, except for some special cases [12,14]. In addition, numerical methods [7], approximate methods [18], or the lambert *W* function [19] can be used to solve the other models [13,15–17]. Numerical methods unavoidably entail cumbersome time-consuming. Approximate methods without doubt introduce large error. Lambert *W* function, as an un-elementary function, is not suitable to be implemented into simulator [20], because there is not method provided to implement all of Lambert *W* function, its differentiation and ingratiation into circuit simulators, such as SPICE or Verilog-A code for models. Therefore, the wide applications and the intensive researches of the new generation solar cells call for the avail solutions of the DC lumped-parameter equivalent circuit models as simple as possible to play an important role on both the applied researches of solar cells and the photovoltaic system simulations. In fact, the most important attribution of our manuscript is deriving the analytical solutions of the reported circuits [7,14,17] to improve the simulation efficiency and giving the detailed discussions about the effects from the model parameters on *I*-*V* curves to complete the groundwork for the further improvement on the reported circuits

\* Corresponding author.

E-mail address: [yufei\\_jnu@126.com](mailto:yufei_jnu@126.com) (F. Yu).

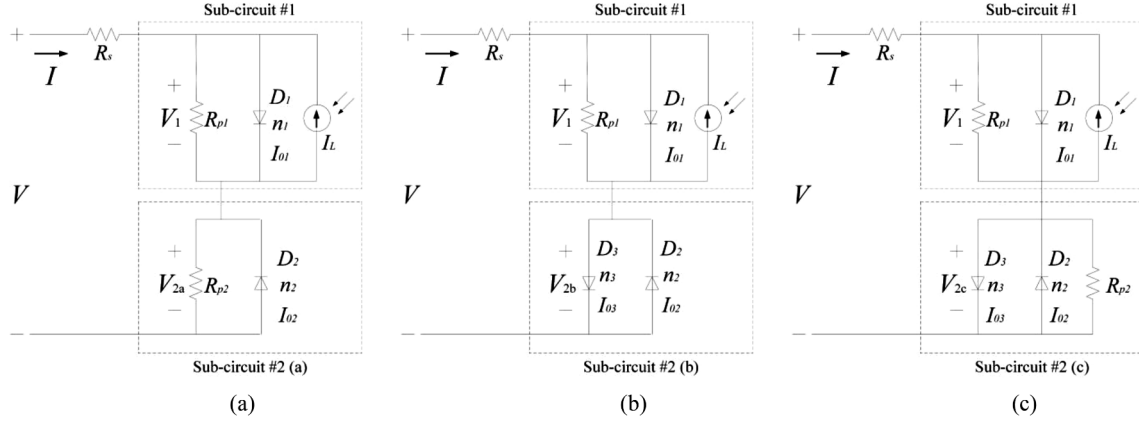


**Fig. 1.** The latest typical solar cells' lumped-parameter equivalent circuit models [7,14,17] adding the sub-circuit #2 into the conventional model sub-circuit #1. (a) The model proposed by F. A. de Castro et al. [7]; (b) The model proposed by F. J. García-Sánchez et al. [14]; (c) The model proposed by P. J. Roland et al. [17].

[7,14,17].

## 2. Models' equation system solution

Since the conventional DC lumped-parameter equivalent circuit models (i.e., sub-circuit #1) cannot describe the S-shaped  $I$ - $V$  characteristics, the latest models [7,14,17] add the ancillary circuits as the sub-circuit #2 to offer a description of solar cells'  $I$ - $V$  characteristics, as shown in Fig. 1.

In the sub-circuit #1 of Fig. 1, a conventional solar cell lumped-parameter model is comprised of the first diode  $D_1$ , the photo-current source  $I_L$ , series resistor  $R_s$ , and shunt resistor  $R_{p1}$ , where  $I_{01}$  is the reverse saturation current of  $D_1$  and  $n_1$  is the ideality factor representing the divergence from the ideal diode. The modified lumped-parameter models usually include an additional series-connected sub-circuit #2 (i) to describe the solar cells' S-shaped  $I$ - $V$  characteristics. In sub-circuit #2 (i), the second diode  $D_{2i}$  with opposite polarity is included to descript the experimentally observed detrimental S-shaped concave region of the illuminated  $I$ - $V$  curve. Here, the letter "i" denotes "a", "b", and "c", respectively. The subscripts "a", "b", and "c" represent the difference of the sub-circuit #2 (a), (b), and (c) in Fig. 1. For the different models (a), (b), and (c), some minor but important modifications are made in the sub-circuit #2. In the sub-circuit #2 (a), the shunt resistor  $R_{p2}$  is used to illustrate the linear control ability for the severity of the anomalous S-shaped kink in the first quadrant. In the sub-circuit #2 (b), the third polarity diode  $D_3$  with ideality factor  $n_3$  and the reverse saturation current  $I_{03}$  replacing  $R_{p2}$  of the sub-circuit #2 (a) describes the exponential-like rise of the anomalous S-shaped kink at the large forward operation voltages. In the sub-circuit #2 (c), the shunt resistor  $R_{p2}$  is connected in parallel with  $D_3$  to simulate bulk transport within the body of solar cells from the phenomenological point of view and control the solar cells'  $I$ - $V$  curve's slope around the origin from the graphical point of view.

According to Fig. 1, the terminal voltage of solar cells can be given by the sum of the voltages of three series-connected parts, i.e.,

$$V = V_R + V_1 + V_{2i} \quad (1)$$

In (1),  $V_R$ ,  $V_1$ , and  $V_{2i}$  are the voltages of the series resister  $R_s$ , sub-circuit #1, and sub-circuit #2 (i), respectively. On the one side, considering that the terminal current flows through two series-connected sub-circuits and  $R_s$ , and the sub-circuit #1 have the same structure in Fig. 1(a), (b), and (c), we can obtain the terminal current  $I$  as the functions of  $V_R$  and  $V_1$  as

$$I = \frac{V_R}{R_s}, \quad (2)$$

$$I = I_{01} \left( e^{\frac{V_1}{n_1 V_t}} - 1 \right) + \frac{V_1}{R_{p1}} - I_L. \quad (3)$$

Here,  $V_t$  is the thermal voltage symbolled by  $kT/q$  where  $k$  is the Boltzmann constant,  $T$  is the absolute temperature, and  $q$  is the electron charge. It is noted that the sun-circuit #1 can be influenced by the illumination, which is represented by (3). On the other side, the sub-circuit #2 (i) has the different structures in Fig. 1(a), (b), and (c). Therefore, we can severally demonstrate the terminal current-voltage functions of sub-circuit #2 (a), (b), and (c), respectively, yielding

$$I = -I_{02} \left( e^{\frac{V_{2a}}{n_2 V_t}} - 1 \right) + \frac{V_{2a}}{R_{p2}}, \quad (4a)$$

$$I = -I_{02} \left( e^{\frac{-V_{2b}}{n_2 V_t}} - 1 \right) + I_{03} \left( e^{\frac{V_{2b}}{n_3 V_t}} - 1 \right), \quad (4b)$$

$$I = -I_{02} \left( e^{\frac{-V_{2c}}{n_2 V_t}} - 1 \right) + I_{03} \left( e^{\frac{V_{2c}}{n_3 V_t}} - 1 \right) + \frac{V_{2c}}{R_{p2}}. \quad (4c)$$

It is noted that the sun-circuit #2 (i) gives the description of the S-shaped kink in the first quadrant for both  $I > 0$  and  $V > V_{oc}$ , which is represented by (4i). Here,  $V_{oc}$  is the open circuit voltage. In fact, the above six functions constitute three transcendental systems including four equations in everyone and having the one-to-one correspondence with the models in Fig. 1(a), (b), and (c), respectively.

Now, by using the Newton-Raphson (NR) method, we can solve the terminal voltages  $V_1$  and  $V_{2i}$  as a function of  $I$  from (3) and (4i), respectively. It is interesting that deriving  $V_1$  and  $V_{2i}$  based on the NR

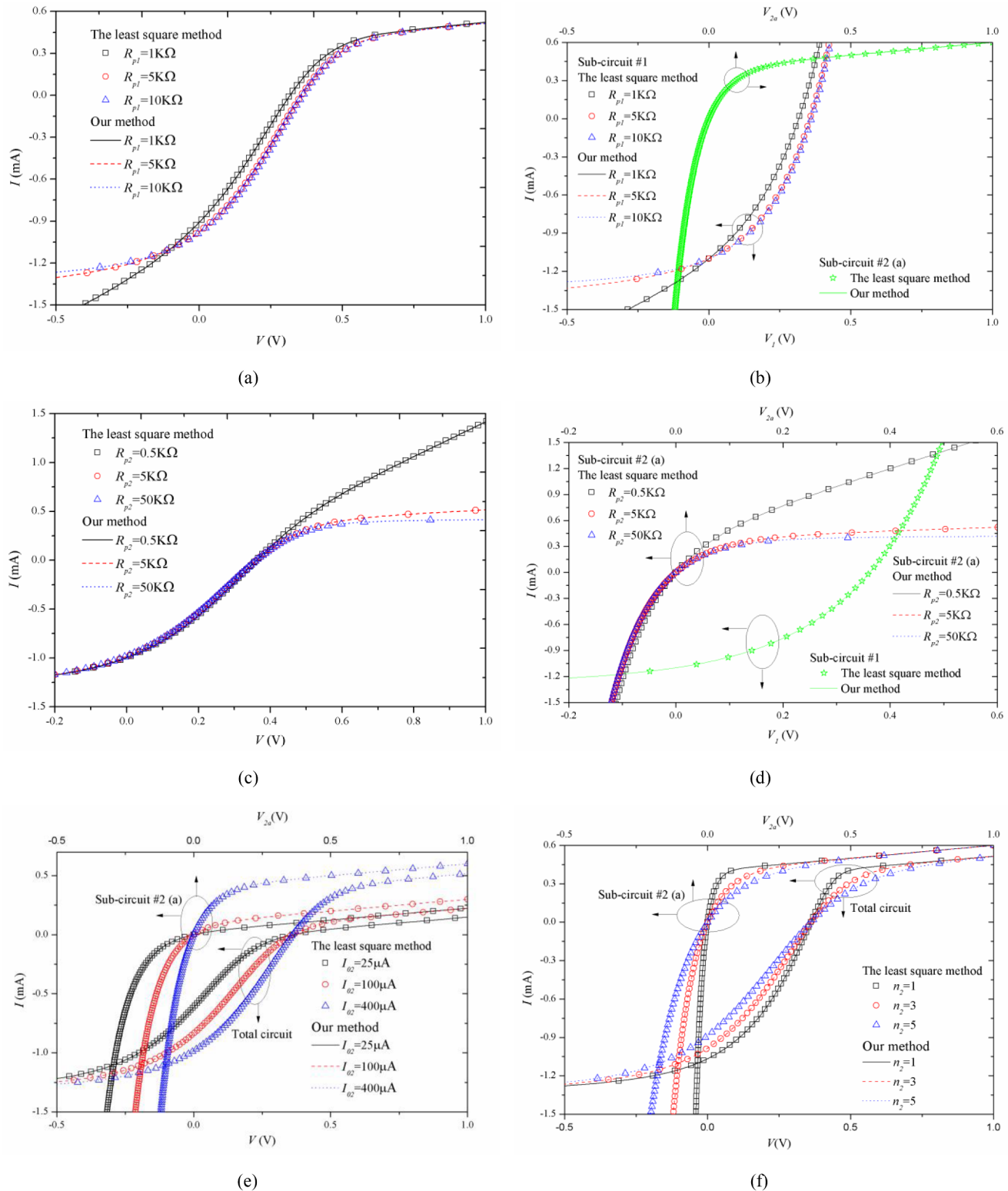


**Fig. 2.**  $I$ - $V$  characteristics in the model of Fig. 1(a). (a) Effects from  $R_{p1}$ ; (b) Effects from  $R_{p1}$  on sub-circuits; (c) Effects from  $R_{p2}$ ; (d) Effects from  $R_{p2}$  on sub-circuits; (e) Effects from  $I_{o2}$ ; (f) Effects from  $n_2$ .

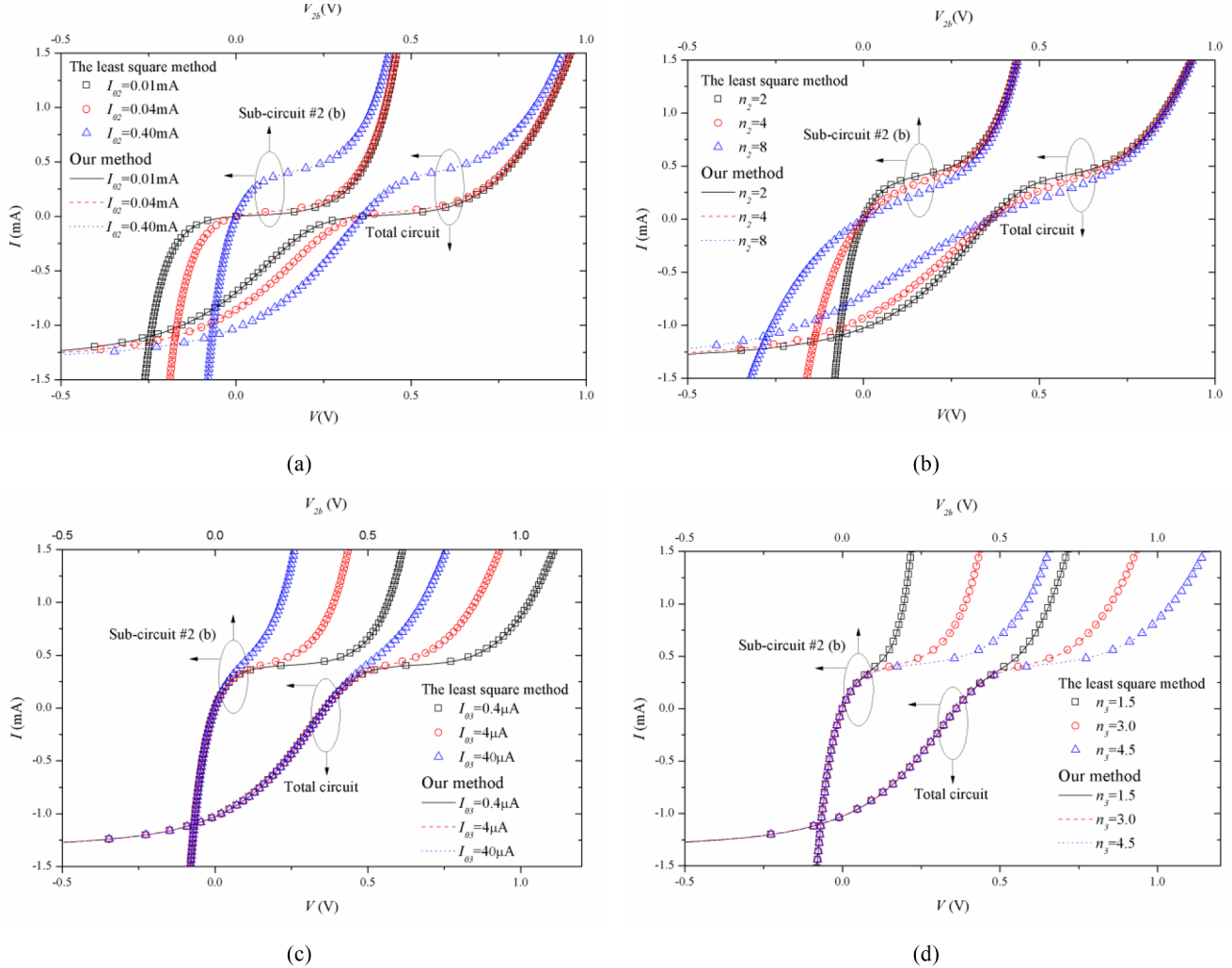


**Fig. 3.**  $I$ - $V$  characteristics in the model of Fig. 1(b). (a) Effects from  $I_{02}$ ; (b) Effects from  $n_2$ ; (c) Effects from  $I_{03}$ ; (d) Effects from  $n_3$ .

method leads to the fast convergences. Practical simulations show that the NR method only require 10–20 iterations to make  $V_1$  and  $V_{2i}$  come into the maximum relative error 5%, which is related to the parameters in the solar cells' lumped-parameter equivalent circuit models. In fact, there is a trade-off between accuracy and efficiency where more iterations lead to higher accuracy of solutions and lower efficiency of computations. It is interesting that this method can effectively decrease time-consuming of solving the models in Fig. 1, compared with the least square method and the lambert  $W$  function widely used in the literatures [7,14,16,17].

### 3. Verification and discussion

We use the least square method to solve the lumped-parameter equivalent circuit models of solar cells shown in Fig. 1(a), (b), and (c). It is noted that  $R_s$  is set as zero to avoid obscuring the comparison. Subsequently, we compare our solutions with the least square method

results to verify the accuracy of our solutions for the different operation conditions, shown in Figs. 2–4. These simulation results demonstrate that our solutions show excellent accuracy of computation in the whole operation regime. The parameters used in simulations are included in Table 1.

For the model proposed by F. A. de Castro et al. [7], we discuss about the influences from the shunt resistor  $R_{p1}$  in the sub-circuit #1 representing the traditional one-diode solar cell model and the other parameters in the sub-circuit #2 (a). Firstly, according to Fig. 2(a) and (b), we can observe that the short-circuit current and open-circuit voltage can be reduced as the decrease of  $R_{p1}$ . In addition, in the case of large  $R_{p1}$ ,  $R_{p1}$  has a little influence on the sub-circuit #1. That is in consist with the structure of the circuit. Secondly, Fig. 2(c) and (d) show the S-shaped illuminated  $I$ - $V$  characteristics for three different shunt resistor  $R_{p2}$  values in the sub-circuit #2 (a). The un-normal S-shaped kink in the first quadrant is controlled by  $R_{p2}$ . We note that  $R_{p2}$  in the sub-circuit #2 (a) describes the linear rise S-shaped kink. Thirdly,

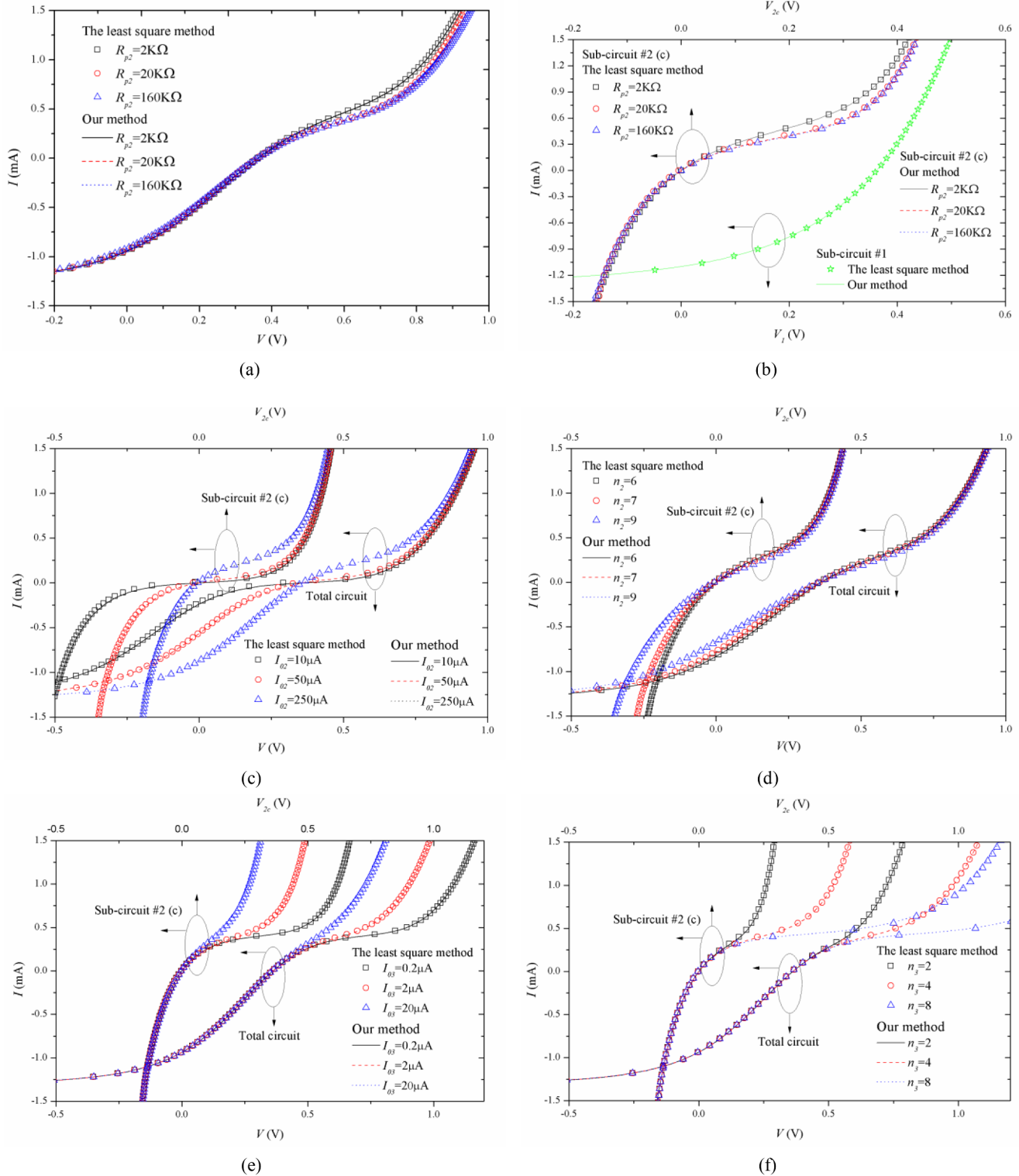


**Fig. 4.**  $I$ - $V$  characteristics in the model of Fig. 1(c). (a) Effects from  $R_{p2}$ ; (b) Effects from  $R_{p2}$  on sub-circuits; (c) Effects from  $I_{o2}$ ; (d) Effects from  $n_2$ ; (e) Effects from  $I_{o3}$ ; (f) Effects from  $n_3$ .

**Table 1**  
Parameters for simulations in Figs. 2–4.

Parameters (Units)	Fig. 2			Fig. 3			Fig. 4						
	(a) (b)	(c) (d)	(e)	(f)	(a)	(b)	(c)	(d)	(a) (b)	(c)	(d)	(e)	(f)
$R_s$ (kΩ)	0	0	0	0	0	0	0	0	0	0	0	0	0
$R_{p1}$ (kΩ)	~	10	10	10	10	10	10	10	10	10	10	10	10
$R_{p2}$ (kΩ)	5	~	5	5	5	5	5	5	~	5	5	5	5
$I_{o1}$ (μA)	140	140	140	140	140	140	140	140	140	140	140	140	140
$I_{o2}$ (μA)	400	400	~	400	~	400	400	400	~	400	400	400	400
$I_{o3}$ (μA)	~	~	~	~	0.4	0.4	~	0.4	0.4	0.4	0.4	~	0.4
$n_1$ (-)	6.5	6.5	6.5	6.5	6.5	6.5	6.5	6.5	6.5	6.5	6.5	6.5	6.5
$n_2$ (-)	3.0	3.0	3.0	~	2.0	~	2.0	2.0	2.0	2.0	~	2.0	2.0
$n_3$ (-)	~	~	~	~	3.0	3.0	3.0	~	3.0	3.0	3.0	3.0	~
$I_L$ (mA)	1.1	1.1	1.1	1.1	1.1	1.1	1.1	1.1	1.1	1.1	1.1	1.1	1.1

**Table 2**  
Parameters for simulations in Fig. 5.

Parameters (Units)	Fig. 5(a)		Fig. 5(b)		Fig. 5(b)	
	Not Annealed	Annealed at 120 °C	Annealed at 150 °C	Annealed at 180 °C	Annealed at 180 °C	Annealed at 200 °C
$R_s$ (kΩ)	0	0	0	0	0	0
$R_{p1}$ (kΩ)	1.87271	1.28702	1.33442	1.42708	1.42708	1.43642
$R_{p2}$ (kΩ)	0.544129	0.297303	~	~	10.5486	0.0476586
$I_{o1}$ (μA)	13.7794	8.37219	20.4833	16.5838	16.5838	29.3955
$I_{o2}$ (μA)	203.105	207.465	502.820	454.319	444.319	902.248
$I_{o3}$ (μA)	~	~	1062.238	3770.33	3770.33	0.873843
$n_1$ (-)	3.01000	3.35130	4.36013	4.17711	4.17711	4.65456
$n_2$ (-)	1.65200	1.24815	1.35009	0.886346	0.886346	1.07165
$n_3$ (-)	~	~	10.0966	10.55000	10.55000	1.83415
$I_L$ (mA)	4.35082	4.16716	14.40866	5.11985	5.11985	5.45468

the reverse current  $I_{o2}$  and the ideal factor  $n_2$  of the second diode  $D_2$  with opposite polarity determine the location of the convexity in the S-shaped anomaly, as shown in Fig. 1(e) and (f).

Fig. 3 shows the simulation results of the model proposed by F. J. García-Sánchez et al. [14]. In Fig. 3(a) and (b), the diode  $D_2$  of the sub-circuit #2 (b) also determines the location of the convexity in the S-shaped anomaly, playing the same role in that of the sub-circuit #2 (a). Here,  $I_{o2}$  and  $n_2$  determine the position and slope of the S-shaped  $I$ -V characteristics in the third quadrant, respectively. In Fig. 3(c) and (d), the forward  $D_3$  the sub-circuit #2 (b) substitutes  $R_{p2}$  of the sub-circuit #2 (a) to make the S-shaped kink rise in the exponential format. Here, analogous with  $I_{o2}$  and  $n_2$ ,  $I_{o3}$  and  $n_3$  also affect the position and slope of the S-shaped kink in the first quadrant, respectively.

In the model proposed by P. J. Roland et al. [17], the shunt resistor  $R_{p2}$  is added in the sub-circuit #2 (c). According to Fig. 4(a) and (b),  $R_{p2}$  is necessary for the bulk transport in solar cells from the phenomenological aspect by slightly controlling the slope of the S-shaped kink from the graphical aspect. In addition, the effects from the parameters of  $D_2$  and  $D_3$  in the sub-circuit #2 (c) are analogous with those in the sub-circuit #2 (b), as shown in Fig. 4(c)–(f).

Furthermore, to validate our proposed method to solve the above presented models, we further compare the simulation results of three models with the reconstructed experimental data [16]. The parameters

used in simulations are included in Table 2. Our solutions also have a good agreement with the reconstructed experimental data [16], as shown in Fig. 5(a)–(c). Moreover, we can observe that the rise of the S-shaped kink changes from the linear to exponential-like as the increase of anneal temperature. That show the significance that the diode  $D_3$  in the sub-circuit #2 (b) is substituted for the resistor  $R_{p2}$  in the sub-circuit #2 (a). In addition, on the condition that the anneal temperature is larger than 180 °C, the shunt resistor  $R_{p2}$  is required to complete fine tuning for the S-shaped kink.

#### 4. Conclusion

In this paper, an analytical solution of the modelling for solar cells with the already proposed lumped-parameter equivalent circuit models has been derived by using the Newton-Raphson method, which can lead to high accuracy and fast convergences. Furthermore, our solutions are verified by using the least square method results and reconstructed experimental data, respectively. Finally, we analyze the effect from the parameters of the models on the solar cells' S-shaped  $I$ -V characteristics. We believe that such an analytical solution could be useful for the electrical explanations on the S-shaped  $I$ -V characteristics and the solar cells' simulations.

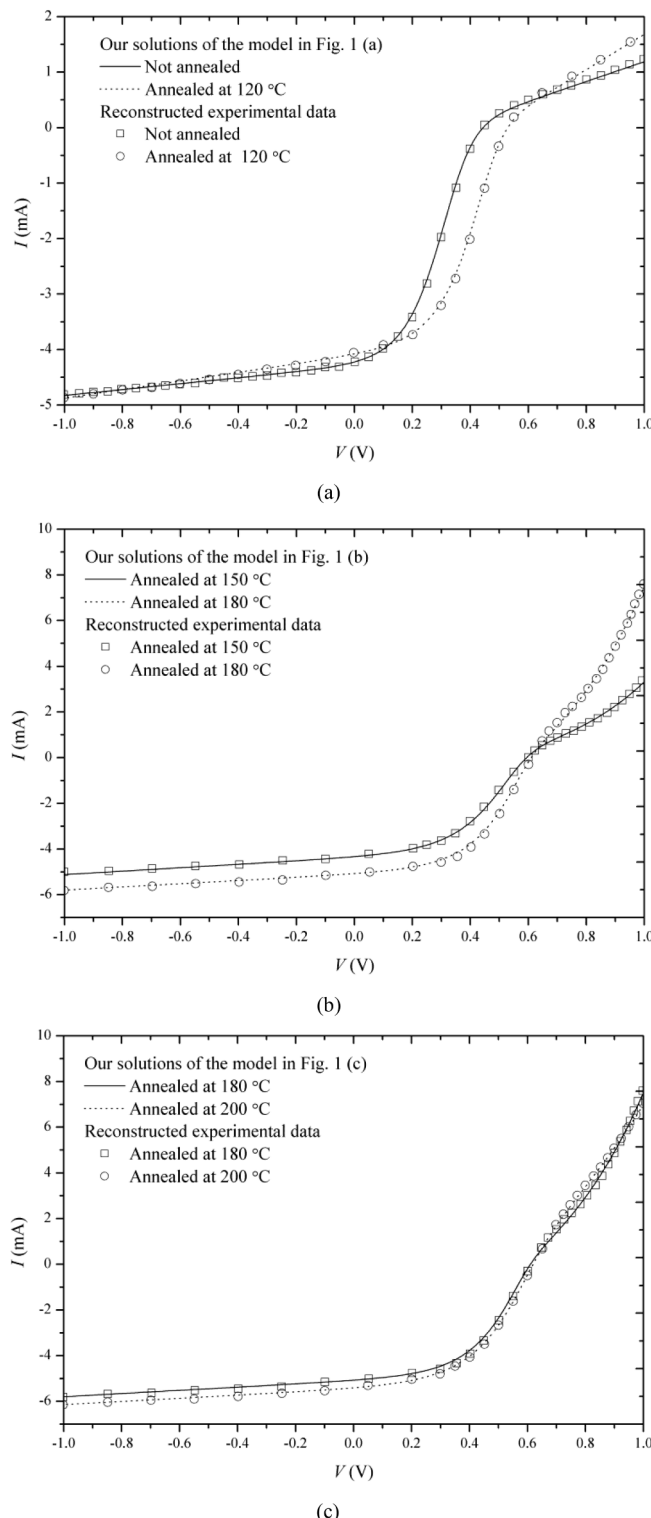


**Fig. 5.** Comparisons between our solutions of the models in Fig. 1 and the reconstructed reconstructed experimental data [16]. (a) The solution of the model in the Fig. 1 (a) vs. the reconstructed experimental data [16]; (b) The solution of the model in the Fig. 1 (b) vs. the reconstructed experimental data [16]; (c) The solution of the model in the Fig. 1 (c) vs. the reconstructed experimental data [16].

## Acknowledgment

This work was funded partially by the Scientific Research Funds of Huaqiao University under grant 16BS706 and partially by the Scientific Research Funds for the Young Teachers of Fujian Province under grant JAT170034.

## References

- Chavali RVK, Li JV, Battaglia C, De Wolf S, Gray JL, Alam MA. A generalized theory explains the anomalous Suns-Voc response of Si heterojunction solar cells. *IEEE J Photovoltaics* 2017;7(1):169–76. <https://doi.org/10.1109/JPHOTOV.2016.2621346>.
- Kale PG, Solanki CS. Silicon quantum dot solar cell using top-down approach. *Int Nano Lett* 2015;5(2):61–5. <https://doi.org/10.1007/s40089-014-0137-0>.
- van Reenen S, Kemerink M, Snaith HJ. Modeling anomalous hysteresis in perovskite solar cells. *J Phys Chem Lett* 2015;6(19):3808–14. <https://doi.org/10.1021/acs.jpclett.5b01645>.
- Xu F, Zhu J, Cao R, Ge S, Wang W, Xu H, et al. Elucidating the evolution of the current-voltage characteristics of planar organometal halide perovskite solar cells to an S-shape at low temperature. *Sol Energy Mater Sol Cells* 2016;157(12):981–8. <https://doi.org/10.1016/j.solmat.2016.08.011>.
- Wagenpfahl A, Rauh D, Binder M, Deibel C, Dyakonov V. S-shaped current-voltage characteristics of organic solar devices. *Phys Rev B* 2010;82(11):115306. <https://doi.org/10.1103/PhysRevB.82.115306>.
- Tran VH, Ambade RB, Ambade SB, Lee SH, Lee IH. Low-temperature solution-processed SnO<sub>2</sub> nanoparticles as cathode buffer layer for inverted organic solar cells. *ACS Appl Mater Interfaces* 2017;9(2):1645–53. <https://doi.org/10.1021/acsami.6b10857>.
- de Castro FA, Heier J, Nuesch F, Hany R. Origin of the kink in current-density versus voltage curves and efficiency enhancement of polymer-C60 heterojunction solar cells. *IEEE J Sel Topics Quantum Electron* 2010;16(6):1690–9. <https://doi.org/10.1109/JSTQE.2010.2040807>.
- Mori H, Miyazaki E, Osaka I, Takimiya K. Organic photovoltaics based on 5-hexylthiophene-fused porphyrazines. *Organic Electron* 2012;13(10):1975–80. <https://doi.org/10.1016/j.orgel.2012.05.023>.
- Wagner J, Gruber M, Wilke A, Tanaka Y, Topczak K, Steindamm A, et al. Identification of different origins for s-shaped current voltage characteristics in planar heterojunction organic solar cells. *J Appl Phys* 2012;111(5):054509. <https://doi.org/10.1063/1.3692050>.
- Qi B, Wang J. Fill factor in organic solar cells. *Phys Chem Chem Phys* 2013;15(23):8972–82. <https://doi.org/10.1039/c3cp51383a>.
- Ortiz-Conde A, Lugo-Muñoz D, García Sánchez FJ. An explicit multi-exponential model as an alternative to traditional solar cell models with series and shunt resistances. *IEEE J Photovoltaics* 2012;2(3):261–8. <https://doi.org/10.1109/JPHOTOV.2012.2190265>.
- Mazhari B. An improved solar cell circuit model for organic solar cells. *Sol Energy Mater Sol Cells* 2006;90(7–8):1021–33. <https://doi.org/10.1016/j.solmat.2005.05.017>.
- Kumar P, Gaur A. Model for the J-V characteristics of degraded polymer solar cells. *J Appl Phys* 2013;113(9):094505. <https://doi.org/10.1063/1.4794356>.
- García-Sánchez FJ, Lugo-Muñoz D, Muci H, Ortiz-Conde A. Lumped parameter modeling of organic solar cells' S-shaped I-V characteristics. *IEEE J Photovoltaics* 2013;3(1):330–5. <https://doi.org/10.1109/JPHOTOV.2012.2219503>.
- Zuo L, Yao J, Li H, Chen H. Assessing the origin of the S-shaped I-V curve in organic solar cells: an improved equivalent circuit model. *Sol Energy Mater Sol Cells* 2014;122(3):88–93. <https://doi.org/10.1016/j.solmat.2013.11.018>.
- De Castro FA, Laudani A, Riganti Fulginei F, Salvini A. An in-depth analysis of the modelling of organic solar cells using multiple-diode circuits. *Sol Energy* 2016;135(10):590–7. <https://doi.org/10.1016/j.solener.2016.06.033>.
- Roland PJ, Bhandari KP, Ellingson RJ. Electronic circuit model for evaluating S-kink distorted current-voltage curves. *Proc. IEEE 43rd Photovoltaic Specialists Conf. (PVSC)* 2016. p. 3091–4. <https://doi.org/10.1109/PVSC.2017.8366732>.
- del Pozo G, Romero B, Arredondo B. Evolution with annealing of solar cell parameters modeling the S-shape of the current–voltage characteristic. *Solar Energy Mater Solar Cells* 2012;104(9):81–6. <https://doi.org/10.1016/j.solmat.2012.04.048>.
- Corless RM, Gonnet GH, GHare DE, Jeffrey DJ, Knuth DE. On the lambert W function. *Adv Comput Math* 1996;5(4):329–59. <https://doi.org/10.1007/BF02124750>.
- Zong Z, Li L, Lu N, Liu M. Analytical surface-potential compact model for amorphous-IGZO thin-film transistors. *J Appl Phys* 2015;117(21):215705. <https://doi.org/10.1063/1.4922181>.



**Fei Yu** received the B.S. degree in Science and Technology College of Nanchang Hangkong University, Nanchang, China, in 2009, and the M.S. and Ph. D. degrees in the Department of Electronic Engineering, Jinan University, Guangzhou, China, in 2013 and 2016, respectively. He is currently working with the College of Information Science and Engineering, Huaqiao University, Xiamen, as a faculty member. His research interests include semiconductor device modeling.



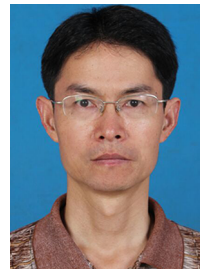
**Wanling Deng** received the B.S. and Ph.D. degrees in electrical engineering from South China University of Technology, Guangzhou, China, in 2003 and 2008, respectively. Since 2008, she has been working with the Department of Electronic Engineering, Jinan University, Guangzhou, as a vice professor. Her research interests include semiconductor devices and physics.



**Gongyi Huang** received the B.S. degree from the Department of Electronic Engineering, the Xi'An JiaoTong University, Xi'An, in 1995. In 1995, he joined the College of Information Science and Engineering, Huaqiao University, Quanzhou, as a faculty member. His current research interests include applications and simulations of solar cells.



**Xiaoyu Ma** received the B.S. degree in Changchun University, Changchun, China, in 2004, and the M. S. degree in Jinan University, Guangzhou, China, in 2006. She is currently pursuing the Ph.D. degree in Jinan University. Her research interests include solar cells' lumped-parameter model.



**Chuanzhong Xu** received the M. S. and Ph.D. degrees in the College of Information Science and Engineering, Huaqiao University, Xiamen, China, in 2004 and 2012, respectively. Since 2004, he has been working in the College of Information Science and Engineering, Huaqiao University, Xiamen. His current research interests include applications and simulations of solar cells.



**Junkai Huang** received the B.S. degree in applied physics and the M. S. degree in semiconductor device from Jinan University, Guangzhou, China, in 1985 and 1990, respectively, and the Ph.D. degree from the Institute of Microelectronics from South China University of Technology, Guangzhou, in 2011. He is currently a Professor with Jinan University. His main research interests include semiconductor device modeling, simulation, and integrated circuit design.